Marine Systems & Ocean Technology (2019) 14:12–22
https://doi.org/10.1007/s40868-018-0051-9

Wave-induced flexural response of idealized non-uniform hull girder in random seas

J. D. Thekinen[1] · **N. Datta**[2]

Received: 25 April 2018 / Accepted: 9 November 2018 / Published online: 26 November 2018

Abstract
The aim is to analyze the wave-induced vertical vibration of a non-prismatic mathematical hull in a stochastic sea, by normal mode analysis. The hull has been generated mathematically, to represent two distinct Indian merchant vessels: DS (Tanker) and SCIM (Containership). The body-plan, deck waterline, bow and stern profiles, have been modeled as semi-superellipses. These render non-uniform distributions of mass and stiffness over the ship-length. The energy-based Rayleigh–Ritz method has been used to analyze the idealized hull girder natural frequencies and modeshapes. The non-uniform beam modeshape is a weighted series sum of prismatic beam-free vibration modeshapes. The 2D added mass of superelliptic sections is formulated, solving the radiation boundary value problem by the constant strength source distribution method. The hull girder is subject to the Pierson–Moskowitz sea spectrum in fully loaded condition. The diffraction force is formulated through the Khaskind's relations. The flexural response of the girder is evaluated by the modal superposition method. The response spectra have been generated for various sea states and ship speeds. The magnitudes of the maximum flexural/shear stress for each vessel are generated. The probability of shear/tensile failure is also estimated, giving insights into the hull structural design.

Keywords Non-uniform beam · Mathematical hull · Rayleigh–Ritz method · Ship springing · Response spectrum

List of symbols

x	Independent variable along length of the hull (m)
$y(x, z)$	Offset from hull centreline (m)
z	Independent variable along the depth of the hull (m)
t	Independent variable in time (s)
$m(x)$	Mass per unit length (kg/m)
$I(x)$	Second moment of cross-section area about horizontal neutral axis (m^4)
E	Modulus of elasticity (N/m)
LOA	Length overall of the hull (m)
L	Length between perpendiculars (m)
B	Moulded breadth (m)
D	Moulded depth (m)
T	Moulded draught (m)
$a(x)$	Local half-breadth (m)
$b(x)$	Local depth (m)
$p(x)$	Rectellipse power (–)
$q(x)$	Rectellipse power (–)
Δ	Displacement (ton)
C_b	Block coefficient (–)
λ	Wavelength of ocean wave (m)
ω_e	Wave circular frequency (rad/s)
J	3D added mass/2D added mass (–)
$a_{j,33}^{2D}(x)$	2D added mass coefficient in heave due to heave associated with jth flexural mode (–)
$z(x, t)$	Vertical flexural displacement of beam (m)
$\Phi_j(x)$	Jth non-uniform beam modeshape (–)
$q_j(t)$	Jth principal coordinate (m/s)
a_{jk}	Weight of the contribution of $\varphi_k(x)$ to $\Phi_j(x)$ (–)
$\varphi_j(x)$	Jth uniform beam modeshape (–)
α_{jk}	Generalized stiffness matrix in Rayleigh–Ritz method
β_{jk}	Generalized mass matrix in Rayleigh–Ritz method
A_0	Material cross-section area of midship section (m^2)
I_0	Vertical second moment of inertia of the midship section (m^4)

✉ N. Datta
nabanitadatta@gmail.com

[1] Department of Mechanical Engineering, Purdue University, West Lafayette, USA

[2] Department of Ocean Engineering and Naval Architecture, Indian Institute of Technology, Kharagpur, India

γ	Spatial frequency of uniform beam vibration (1/m)
ρ	Material density (kg/m^3)
$\Psi_3(x,z,t)$	2D heave radiation potential (m^2/s)
$b_{33}^{2D}(x)$	2D radiation damping coefficient in heave due to heave associated with jth flexural mode (–)
$G_{PQ}(y,z;\xi,\eta)$	2D constant strength Green's function between field point P and source point Q
$P(y,z)$	Field point (–)
$Q(\xi,\eta)$	2D source point (–)
$r_{PQ,n}$	Distance between P and nth source Q (m)
ω_j	Jth natural frequency of non-uniform beam (rad/s)
$\psi_j(x,z)$	Jth auxiliary radiation potential (m)
$\psi_0(x,z,t)$	2D incident wave potential (m^2/s)
$\psi_D(x,z,t)$	Wave diffraction potential (m^2/s)
ζ	Wave amplitude (m)
k	Wave number of incident wave (1/m)
$S(\omega_e)$	Sea spectrum ordinate
$\Psi_3(x,z,t)$	2D radiation potential due to heave (m^2/s)
GM_{jk}	Generalized mass in mode summation method
GA_{jk}	Generalized added mass in mode summation method
GK_{jk}	Generalized stiffness in mode summation method
$M(x,t)$	Bending moment (N-m)
$V(x,t)$	Shear force (N)
$\sigma_{xx}(x,t)$	Normal stress (N/m^2)
$\sigma_{xx}(x,t)$	Shear stress (N/m^2)
T_z	Average zero-up crossing period (s)
$H_{1/3}$	Significant wave height (m)
θ	Heading angle (rad)
ω_{enc}	Wave encounter frequency (rad/s)
V	Ship speed (m/s)
g	Acceleration due to gravity (m/s^2)
N	Number of waves (–)
$p(\sigma_{amp})$	Probability density of normal stress amplitude (–)

1 Introduction

Investigation of hull vibration has become increasingly important due to marine structures becoming longer and larger. Global, steady-state, lightly damped, lower-frequency-higher-amplitude vibrations of the ship hull girder, called springing, lead to global bending and shear stresses, and high-cycle fatigue. The hull girder's natural period in a typical merchant ship is of the range 0.5–3 s. Typical ocean wave period is 8–20 s. However, the strongest wave-bending moments on the hull are caused when the wave length equals the ship length, which corresponds to a low frequency of $\omega \sim 0.5$ rad/s. Also, forward speeds of the ship stretch the frequency domain on the higher frequency end (lowering the excitation period), causing the excitation frequency and natural frequency to approach each other, predisposing the hull girder to a resonant excitation by the ocean waves.

Troesch [1] studied the wave-induced hull vibrations both theoretically and experimentally, but the springing modeshape was highly simplified to a piece-wise rigid-body mode. This work generated the normalized springing response spectrum for different Froude numbers of the Great Lakes bulk carrier model. Newman [2, 3] studied the bending of a slender barge, a vertical column, hinged barge, and the wave effects in a channel. The 2D boundary value problem in radiation–diffraction was set up, for both the rigid-body and flexural radiation potentials. However, the structure remained uniform. Jensen [4] detailed the study of short-term and long-term statistics of wave-induced non-prismatic Timoshenko hull vibration bending moments and shear forces in stochastic seaways, using quadratic strip theory. Jung et al. [5] used the quadratic strip theory to calculate the non-linear radiation and diffraction forces, and then estimate vertical, horizontal, and torsional bending moments both analytically and numerically. Wu and Moan [6] studied the same both analytically and experimentally, inclusive of the dynamic effects like slamming. Kim et al. [7] numerically studied springing coupled with the rigid body modes with fully coupled CFD-FEM analysis. It used the higher-order Rankine-panel method. This computationally expensive analysis is limited to the time domain only. Zhu et al. [8] experimentally analyzed bending and torsional hull vibrations using a backbone model. This is again an expensive and long process, bypassing the mathematical rigor.

In this work, the merchant ship hull is modeled mathematically with superellispes, replicating the standard body plan of a typical containership and a tanker. The vertical-plane vibration frequencies and modeshapes are generated. The non-uniform beam modeshape is a series superposition of the uniform beam. Strip theory and Ritz method are used to generate the wet vibration natural frequency. The non-uniform girder is subjected to the deep water waves, represented in the frequency domain by the unidirectional PM spectrum. Linear potential theory is used, with the hydrodynamic pressure acting on the mean wetted surface area. Assuming strip theory, the 2D radiation potential for each station is solved by the Green's function technique. It utilizes the body boundary condition of the velocity of the fluid at the surface of the body equals the structural velocity. Added mass distributions corresponding to all the modeshapes have been distinctly calculated. The diffraction potential is expressed in terms of the radiation potential, through the Khaskind's relation, and the no-penetration body boundary condition of the excitation potential. Normal mode summation method is

used to generate the dynamic deflections in space and time, giving the tensile and shear stress in both the time domain and frequency domain. The response spectra is used to predict the extreme stress magnitudes than can occur at least once during a typical voyage duration.

2 Problem formulation

The merchant ship hull is modeled as a non-uniform free–free Euler–Bernoulli beam, with arbitrarily varying mass and stiffness distributions $m(x)$ kg/m and EI(x) N/m^2. The mass and stiffness distributions do not vary mathematically, unlike in [9]. Table 1 gives the main particulars of the two vessels (a) container ship and the (b) tanker. The body plans of the two vessels are given below in Fig. 1. The 'x'-coordinate is from the Aft perpendicular (AP) towards the Fore perpendicular (FP), the 'y'-coordinate is transverse towards the starboard, and 'z' is vertically upwards. The bench-mark hulls are symmetric fore and aft.

The non-uniform hull is first modeled as a benchmark case of analytical definition, with the same principal dimensions. The container ship is benchmarked as a semi-ellipsoid, obeying the equation $\left(\frac{x}{\text{LOA}/2}\right)^2 + \left(\frac{y}{B/2}\right)^2 + \left(\frac{z}{D}\right)^2 = 1$, and the tanker is benchmarked as a semi-superellipsoid, obeying the equation $\left(\frac{x}{\text{LOA}/2}\right)^4 + \left(\frac{y}{B/2}\right)^4 + \left(\frac{z}{D}\right)^4 = 1$, where LOA is the overall length of the hull, B is the moulded breadth, and D is the moulded depth.

The container and tanker are modeled with rectelliptic sections in the body plan (Fig. 1), i.e., each section obeys the equation $\left(\frac{y}{a(x)}\right)^{p(x)} + \left(\frac{z}{b(x)}\right)^{q(x)} = 1$.Here, $a(x)$ is the local half-breadth and $b(x)$ is the local depth of the station, both of which vary (piece-wise) superelliptically to generate a finer fore and a fuller stern. For the requisite bilge radius, we need $p, q = 14 - 16$ at the midship station. For the flared sections at the fore, we require $p > 1$, $q < 1$. For the stations in the aft, $p < 1$, $q > 1$ are required to accommodate the stern tube. The steel mass distribution $m(x)$ and stiffness EI(x) distribution of the four hulls are given below in Fig. 2. The cargo adds to the inertia without affecting the flexural rigidity of the hull girder, and hence, the loaded ship has a larger natural period.

Table 1 Main particulars of case-study and bench-mark vessels

Particulars	Unit	SCIM container	DS tanker	Semi-ellipsoid	Semi-rectellipsoid
LOA	m	262	249.98	262	249.98
L	m	248	239	248	239
B	m	32.2	44	32.2	44
D	m	19.5	21.5	19.5	21.5
T	m	13.2	15.1	19.5	21.5
L/B	–	7.70	5.43	7.70	5.43
B/T	–	2.44	2.91	2.44	2.91
Disp Δ	ton	74,660	136,011		
C_b	–	0.708	0.856	0.523	0.835
$\lambda = L$	m	248	239	248	239
ω	rad/s	0.498	0.508	0.498	0.507
J factor	–	0.8087	0.7224	0.8087	0.7224

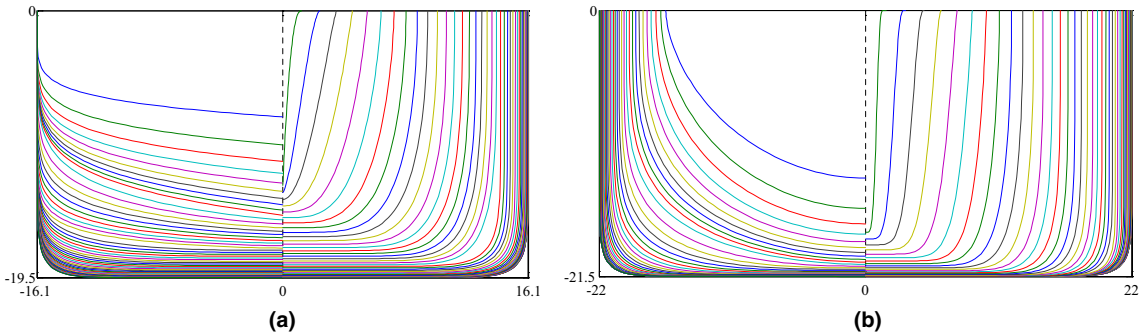

Fig. 1 **a** Containership mathematical body plan, **b** tanker mathematical body plan

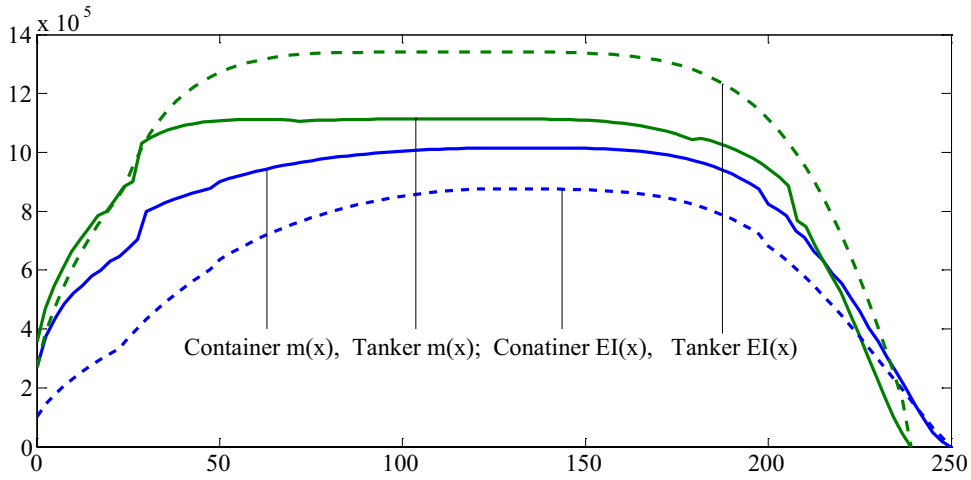

Fig. 2 Mass $m(x)$, flexural rigidity $\mathrm{EI}(x)\times 10^{-8}$ distribution

3 Analysis methodology

The free vibration analysis is done to establish the dry natural frequencies and modeshapes. The details of the dry vibration analysis are shown in detail by the authors in Datta and Thekinen [10]. The modeshapes are used to generate the jth added mass distribution $a^{2D}_{j,33}(x)$. It is the 2D added mass (kg/m) per unit length in heave (subscript 3) due to heave (subscript 3). This leads to the wet natural frequencies, lower than their dry counterparts.

3.1 Free dry vibration

The out-of-plane flexural displacement of the non-uniform Euler–Bernoulli beam in the vertical plane $z(x,t)$ obeys the governing differential equation (GDE)

$$m(x)\frac{\partial^2 z(x,t)}{\partial t^2}+\frac{\partial^2}{\partial x^2}\left\{\mathrm{EI}(x)\frac{\partial^2 z(x,t)}{\partial x^2}\right\}=0. \tag{1}$$

Assuming small-amplitude displacements where linear superposition holds, the total displacement $z(x,t)$, can be assumed to be a superposition of the modal displacements

$$z(x,t)=\sum_{j=1}^{\infty}\Phi_j(x)q_j(t), \tag{2}$$

where $\Phi_j(x)$ is the jth non-uniform beam modeshape and $q_j(t)$ is the jth principal coordinate. Here $\Phi_j(x)$ is the non-uniform beam mode, which is a weighted sum of the admissible functions, i.e.,

$$\Phi_j(x)=\sum_{k=1}^{\infty}a_{jk}\varphi_k(x), \tag{3}$$

where is the closed-form uniform beam modeshape with free–free end condition, and is the weight of the contribution of the kth uniform beam modeshape to the jth non-uniform beam modeshape Table 2. Here, acts as the jth admissible function to the series sum Eq. 3, and satisfies the boundary conditions, i.e., shear force and the bending moment are zero at the ends, i.e.,

$$\begin{aligned}&\mathrm{EI}(0)\Phi_j''(0)=0,\quad \mathrm{EI}(L)\Phi_j''(L)=0,\\&\mathrm{EI}(0)\Phi_j'''(0)=0,\quad \mathrm{EI}(L)\Phi_j'''(L)=0.\end{aligned} \tag{4}$$

Putting the generalized stiffness and mass, respectively, as

$$\alpha_{jk}=\int_0^L\varphi_j''(x)\varphi_k''(x)\mathrm{d}x;\quad \beta_{jk}=\int_0^L\varphi_j(x)\varphi_k(x)\mathrm{d}x, \tag{5}$$

and applying the Ritz method as explained in [9], the equation

$$\sum_{k=1}^{N}a_j\left(\alpha_{jk}-\gamma\beta_{jk}\right)=0, \tag{6}$$

Table 2 Weighted contribution and frequencies

j	Container					Tanker				
	a_{j1}	a_{j2}	a_{j3}	a_{j4}	$\omega_{j\mathrm{ND}}$	a_{j1}	a_{j2}	a_{j3}	a_{j4}	$\omega_{j\mathrm{ND}}$
1	1	−0.14	−0.12	0.02	23.36	−1	−0.12	−0.12	0.02	27.74
2	0.07	1	0.06	0.03	45.13	−0.06	1	0.03	−0.003	54.29
3	0.012	0.02	−1	0.02	72.00	0.002	0.001	−1	−0.01	86.83
4	0.002	0.08	−0.01	−1	108.0	−0.01	0.04	0.02	−1	130.3

is solved for 'j' number of equations. It aims to minimize the frequency by assuming a certain modeshape. The natural frequency of beam vibration,$\omega_j = \gamma^2\sqrt{\frac{\mathrm{EI}_0}{\rho A_0}}$, where I_0 is the vertical second moment of inertia of the midship section, and A_0 is its area. The non-dimensional frequency $\omega_{j\mathrm{ND}}$ is obtained by diving the frequency by $\sqrt{\frac{\mathrm{EI}_0}{\rho L^4 A_0}}$. The non-uniform beam modes (Fig. 3a) are not orthogonal to each other (Table 3). The inner product of the non-uniform mode is:

$$\int_{x=0}^{x=L} \Phi_j(x)\Phi_k(x)\mathrm{d}x = \sum_{l=1}^{\infty} {a_{ll}}^2 \quad \text{if} \quad j = k$$

$$\text{and} \quad \int_{x=0}^{x=L} \Phi_j(x)\Phi_k(x)\mathrm{d}x = \sum_{l=1}^{\infty} a_{jl}\, a_{kl}$$

$$\text{if} \quad j \neq k$$

A convergence study (Fig. 3b) has been done to ensure that enough $\varphi_k(x)$ in Eq. (3) are used to satisfactorily define $\Phi_j(x)$. Here, the first five uniform modes are included to generate the non-uniform mode.

3.2 Free wet vibration

Obeying Newton's second law in the vertical direction, the GDE of free vibration in fluid is given as:

$$m(x)\frac{\partial^2 z(x,t)}{\partial t^2} + \frac{\partial^2}{\partial x^2}\left\{\mathrm{EI}(x)\frac{\partial^2 z(x,t)}{\partial x^2}\right\} = \int -\rho\frac{\partial \Psi_3(x,y,z,t)}{\partial t}\hat{\boldsymbol{k}}\cdot\hat{\boldsymbol{n}}|\mathrm{d}l| \,. \tag{7}$$

The RHS of Eq. 7 is the radiation force at that section. When the ship vibrates in its vertical mode, each individual station heaves with respect to each other, according to the shape of the beam modes. Linear strip theory is assumed, with each vertical section hydrodynamically independent of each other. The total 2D heave radiation potential $\Psi_3(x,z,t)$ associated with the individual 2D boundary value problem in heave,

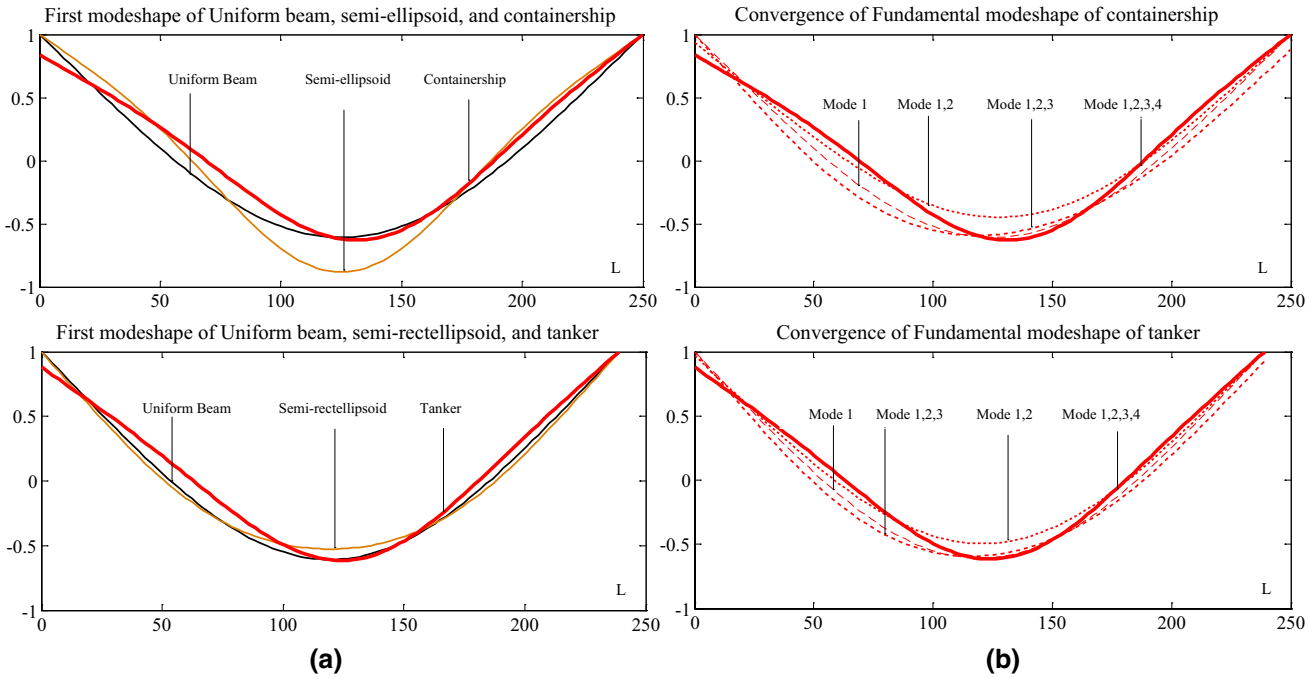

Fig. 3 **a** Fundamental modeshapes along length of the hull L. **b** Convergence of first modeshape along length of the hull L

Table 3 Inner product of non-uniform modeshapes

k	Container				Tanker			
	1	2	3	4	1	2	3	4
1	56.33	−4.81	7.16	−1.65	52.97	−4.77	6.54	−1.27
2	−4.81	51.98	−1.86	2.75	−4.77	58.55	−1.99	2.48
3	7.16	−1.86	59.12	−0.70	6.54	−1.99	64.91	−0.49
4	−1.65	2.75	−0.70	72.62	−1.27	2.48	−0.49	68.34

for each station, generates the added mass $a_{33}^{2D}(x)$ and damping coefficients $b_{33}^{2D}(x)$. The high-frequency vibration generates a rigid-lid condition, without any radiated waves, such that the wave damping coefficient $b_{33}^{2D}(x) \to 0$. It becomes a double-body problem, with the body behaving as though oscillating in an infinite fluid. The radiation potential can be solved by the 2D Green's function technique, by distributing constant-strength sources on the wetted surface and its reflection. The 2D Green's function is:

$$G_{PQ}(y,z;\xi,\eta) \equiv \sum_{n=1}^{2N} \frac{1}{2\pi} \ln\left(r_{PQ,n}\right), \tag{8}$$

where $P(y,z)$ is the field-point and $Q(\xi,\eta)$ is the source-point, and where $r_{PQ,n}$ is the distance between P and nth source Q. N sources are distributed on the wetted perimeter of that station, and there are another N image sources due to reflection. The $\Psi_3(x,z,t)$ on the surface of the body, at a given x -location, is

$$\frac{1}{2}\Psi_3(y,z,t) = \int \left[\Psi_3(\xi,\eta,t)\frac{\partial G_{PQ}(y,z;\xi,\eta)}{\partial \hat{\boldsymbol{n}}} - G_{PQ}(y,z;\xi,\eta)\frac{\partial \Psi_3(\xi,\eta,t)}{\partial \hat{\boldsymbol{n}}}\right]\hat{\boldsymbol{n}}|\mathrm{d}l|. \tag{9}$$

The body boundary condition (BC) of no-penetration, i.e., the normal velocity is continuous, is expressed as

$$\frac{\partial \Psi_3(y,z,t)}{\partial \hat{\boldsymbol{n}}} = \sum_{j=1}^{\infty} \Phi_j(x)\dot{q}_j(t)\hat{\boldsymbol{k}}\cdot\hat{\boldsymbol{n}} \quad \Rightarrow \quad \sum_{j=1}^{\infty} \frac{\partial \Psi_{j3}(y,z,t)}{\partial \hat{\boldsymbol{n}}} = \sum_{j=1}^{\infty} \Phi_j(x)\dot{q}_j(t)\hat{\boldsymbol{k}}\cdot\hat{\boldsymbol{n}}. \tag{10}$$

Here, $\Psi_{j3}(y,z,t)$ is the jth radiation potential satisfying the GDE $\nabla^2\Psi_{3,j}(y,z,t) = 0$. Defining $\Psi_{j3}(y,z,t)$ per unit jth body velocity $\Phi_j(x)\dot{q}_j(t)$, i.e.,

$$\Psi_{3,j}(x,z,t) \equiv \psi_j(x,z)\Phi_j(x)\dot{q}_j(t) \tag{11}$$

we get $\psi_j(x,z)$ which is called the auxiliary radiation potential. Thus, Eq. 10 becomes

$$\sum_{j=1}^{\infty} \frac{\partial \psi_j(x,z)}{\partial \hat{\boldsymbol{n}}} \Phi_j(x)\dot{q}_j(t) = \sum_{j=1}^{\infty} \Phi_j(x)\dot{q}_j(t)\hat{\boldsymbol{k}}\cdot\hat{\boldsymbol{n}}. \tag{12}$$

The jth body BC becomes $\frac{\partial \psi_{j3}}{\partial \hat{\boldsymbol{n}}} = \hat{\boldsymbol{k}}\cdot\hat{\boldsymbol{n}}$, which is time-independent. Thus the radiation force in Eq. (7) is expressed as

$$\int -\rho i\omega \Psi_3(x,y,z,t)\hat{\boldsymbol{k}}\cdot\hat{\boldsymbol{n}}|\mathrm{d}l| = \sum_{j=1}^{\infty} \int -\rho\psi_j(x,z)\Phi_j(x)\ddot{q}_j(t)\frac{\partial \psi_{3,j}(x,z)}{\partial \hat{\boldsymbol{n}}}. \tag{13}$$

This term is a vertical force in phase with the structural acceleration, which can be taken on the LHS of (Eq. 7) to represent the added mass of the jth mode. The J factor has been included, i.e., the ratio of the 3D fluid kinetic energy to the 2D fluid kinetic energy. It accounts for the three-dimensional flow around the ends of the hull girder, and depends on the length-to-beam (L/B) ratio.

Figure 4 shows the sectional radiation force per unit structural acceleration (Eq. 12) for the four hulls: idealized containership, idealized tanker, ellipsoid, and rectellipsoid. The distribution approximately follows the fundamental modeshape of the hull girder. It also depends on the section shape and perimeter, and hence goes to zero at the two ends. The tanker has a higher sectional radiation force than the containership due to a larger sectional area.

Figure 5 shows the non-dimensional frequency parameter $\omega_{j\mathrm{ND}} = \omega_j / \sqrt{\frac{\mathrm{EI}_0}{\rho L^4 A_0}}$, both dry and wet, for the four hulls. For

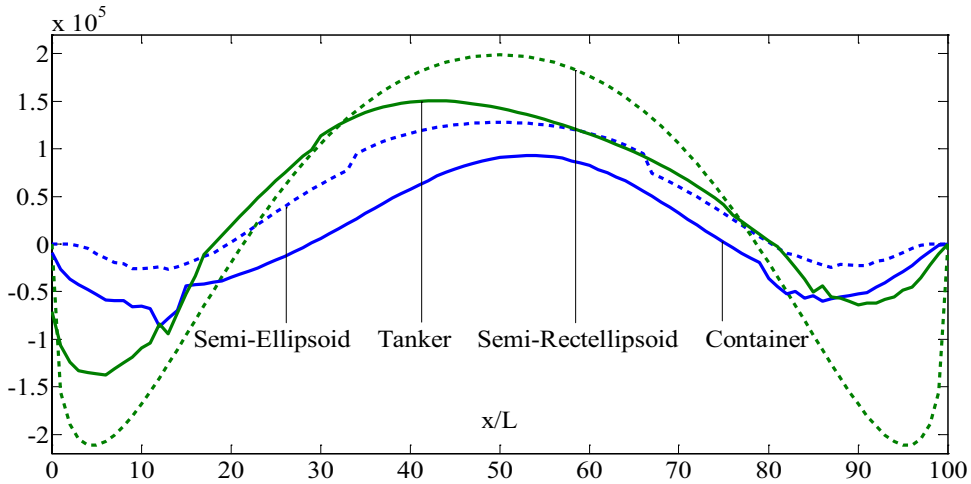

Fig. 4 Added mass distribution $m(x)$ ton/m

a uniform free–free beam, the fundamental frequency parameter $(\gamma L)^2$ is $(4.73)^2 = 22.37$; the second frequency parameter $(\gamma L)^2$ is $(7.85)^2 = 61.62$; the third frequency parameter $(\gamma L)^2$ is $(10.99)^2 = 120.9$; and the fourth frequency parameter $(\gamma L)^2$ is $(14.14)^2 = 199.7$. The dry $\omega_{j\mathrm{ND}}$ of the non-uniform beam is less than that of the uniform beam since the frequency is non-dimensionalized by a larger parameter $\sqrt{\frac{\mathrm{EI}_0}{\rho L^4 A_0}}$, where I_0 and A_0 are measured at the midship and hence the largest in magnitude compared to those at other sections.

Table 4 shows the %age drop in the natural frequency due to inclusion of fluid inertia, which reduces with increasing mode. The fundamental mode shows the highest drop (~60%) in the frequency. The fourth mode has a drop of only ~33%. This is due to increased opposite antinodes for higher beam wave numbers, which partially cancel out the fluid inertia.

Table 4 %Age drop in wet frequency from the dry frequency $\left(\frac{\omega_{\mathrm{dry}}-\omega_{\mathrm{wet}}}{\omega_{\mathrm{dry}}} \times 100\right)$

Mode	Ellipsoid	Rectellipsoid	Container	Tanker
1	56.8	63.2	61.6	61.5
2	51.9	48.8	49.5	49.8
3	37.9	39.1	37.2	38.8
4	34.3	33.2	33.8	34.2

3.3 Forced vibration

The non-uniform beam is subject to the Pierson–Moskowitz spectrum. The 2D incident wave potential in deep water is $\psi_0(x,z,t) \equiv \frac{\zeta g}{\omega} e^{kz} e^{i(kx-\omega_e t)}$; where, ω_e is the excitation frequency, ζ is the amplitude, and k is the wave number of the external waves. If the full-developed zero-mean, stationary and ergodic sea spectrum is expressed as $S(\omega_\mathrm{e})$, the amplitude is $\zeta(\omega_\mathrm{e}) = \sqrt{2 \int_{\omega-\mathrm{d}\omega/2}^{\omega+\mathrm{d}\omega/2} S(\omega_\mathrm{e})\mathrm{d}\omega_\mathrm{e}}$. The deep water dispersion relation is $\omega_\mathrm{e}^2 = gk$, which gives the wave number 'k'. The nth moment of the sea spectrum is given as $m_n = \int_0^\infty \omega_\mathrm{e}^n S(\omega_\mathrm{e})\mathrm{d}\omega$. The total excitation potential is $\psi_{\mathrm{excitation}}(x,z,t) = \psi_0(x,z,t) + \psi_D(x,z,t)$, i.e., the incident wave potential and the diffraction potential.

The linear hydrodynamic force, including the diffraction force, is expressed as

$$F(x,z,t) \equiv \int -\rho \frac{\partial \Psi_0 + \Psi_D]}{\partial t} \hat{\boldsymbol{k}} \cdot \hat{\boldsymbol{n}} |\mathrm{d}l|. \tag{14}$$

To satisfy the body boundary condition of "no-penetration" in a diffraction problem (when the body is supposed to be stationary), $\frac{\partial \psi_0}{\partial \hat{\boldsymbol{n}}}(x,z,t) = -\frac{\partial \psi_\mathrm{D}}{\partial \hat{\boldsymbol{n}}}(x,z,t)$ holds true. The total excitation force is :

$$\begin{aligned} F(x,t) &\equiv \int -\rho i \omega_\mathrm{e} [\Psi_0 + \Psi_\mathrm{D}] \hat{\boldsymbol{k}} \cdot \hat{\boldsymbol{n}} |\mathrm{d}l| \\ &= \int -\rho i \omega_\mathrm{e} [\Psi_0 + \Psi_\mathrm{D}] \frac{\partial \psi_{j3}}{\partial \hat{\boldsymbol{n}}} |\mathrm{d}l|. \end{aligned} \tag{15}$$

The diffraction potential can be expressed in terms of the radiation potential $\Psi_3(x,z,t)$.The jth excitation force is:

$$F_j(x,z,t) = \int -\rho i \omega_\mathrm{e} \left\{ \Psi_0 \frac{\partial \Psi_{3,j}}{\partial \hat{\boldsymbol{n}}} - \Psi_{3,j} \frac{\partial \Psi_0}{\partial \hat{\boldsymbol{n}}} \right\} |\mathrm{d}l|, \tag{16}$$

by the Haskind's relation, using the Green's second identity, as detailed in [11]. The Haskind's relation gives the total wave excitation force, i.e., the incident and diffraction forces, in terms of the incident and radiation potentials, as follows :

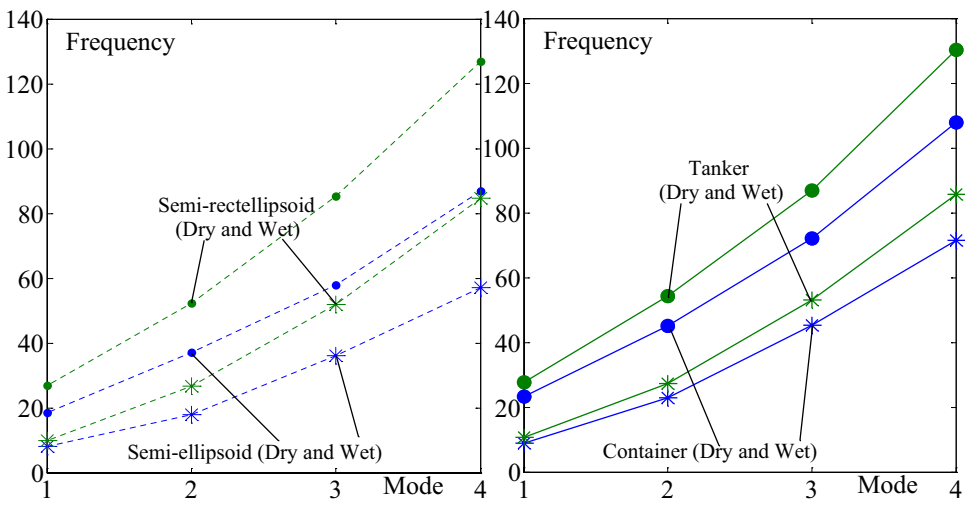

Fig. 5 Dry vs. wet non-D frequency $\omega_{j\mathrm{ND}} = \omega_j / \sqrt{\frac{\mathrm{EI}_0}{\rho L^4 A_0}}$ for the idealized hulls and their fore-aft symmetric counterparts

$$F_{\text{excitation}}(x,z;t) = -\rho \iint_{S_B} \left\{ \frac{\partial \phi_0}{\partial t} + \frac{\partial \phi_D}{\partial t} \right\} dS$$
$$= \rho \iint_{S_B} \left\{ \phi_0 \frac{\partial \phi_3}{\partial n} - \phi_3 \frac{\partial \phi_0}{\partial n} \right\} \mathrm{d}S. \tag{17}$$

The first part is the Froude–Krylov force and the second part is the diffraction force. The forced wet vibration GDE of motion of non-uniform beam is given as

$$m(x)\frac{\partial^2 z(x,t)}{\partial t^2} + \frac{\partial^2}{\partial x^2}\left\{ \mathrm{EI}(x)\frac{\partial^2 z(x,t)}{\partial x^2} \right\}$$
$$= \int -\rho i\omega_e \Psi_3(x,y,z,t)\hat{\boldsymbol{k}} \cdot \hat{\boldsymbol{n}} |\mathrm{d}l| \tag{18}$$
$$+ \int -\rho i\omega_e \left[\Psi_0 \frac{\partial \Psi_3}{\partial \hat{\boldsymbol{n}}} - \Psi_3 \frac{\partial \Psi_0}{\partial \hat{\boldsymbol{n}}} \right] |\mathrm{d}l| .$$

The RHS has the first term as the radiation force, and the second term as the excitation force. Figure 6 shows the excitation force as a function of space and time, for sea state 7 (Beaufort scale).

3.3.1 Mode superposition method

Equation (18) is solved by the mode-summation method, by first generating the system of modal governing differential equations. The generalized mass $\boldsymbol{GM}_{jk}$, generalized added mass $\boldsymbol{GA}_{jk}$, generalized stiffness $\mathbf{GK}_{jk}$ matrices are all non-diagonal, yet symmetric.

$$\boldsymbol{GM}_{jk} = \int_L \Phi_k(x) m(x) \Phi_j(x) \mathrm{d}x;$$
$$\boldsymbol{GA}_{jk} = \int_L -\rho \psi_j(x,z) \Phi_k(x) \Phi_j(x) \frac{\partial \psi_{3,j}(x,z)}{\partial \hat{\boldsymbol{n}}} \mathrm{d}x,$$
$$\boldsymbol{GK}_{jk} = \int_L \mathrm{EI}(x) \Phi_j''(x) \Phi_k''(x) \mathrm{d}x. \tag{19}$$

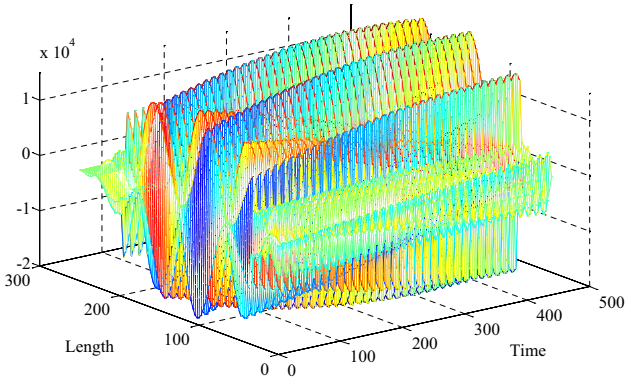

Fig. 6 Excitation force, sea state 7 (Wind speed = 14–17 m/s, $H_{1/3}$ = 4–5.5 m)

The generalized force is given as:

$$\mathbf{GF_k}(t) = \int_L \Phi_k(x) \left\{ \int -\rho i\omega_e \left\{ \Psi_0 \frac{\partial \Psi_3}{\partial \hat{\boldsymbol{n}}} - \Psi_3 \frac{\partial \Psi_0}{\partial \hat{\boldsymbol{n}}} \right\} |\mathrm{d}l| \right\} \mathrm{d}x$$
$$= GF_k(t) e^{-i\omega_e t} . \tag{20}$$

Thus the modal equations become

$$[[\boldsymbol{GM}] + [\boldsymbol{GA}]]\{\ddot{q}_k(t)\} + [\mathrm{GK}]\{q_k(t)\} = \mathbf{GF_k}(t) \quad \Rightarrow$$
$$\{q_k(t)\} = \frac{\{GF_k(t)\mathrm{e}^{-i\omega_e t}\}}{\left[[\mathrm{GK}] - \omega_e^2 ([\boldsymbol{GM}] + [\boldsymbol{GA}])\right]} \tag{21}$$
$$\tag{21}$$

Equation (21) is time-integrated by the stable Euler's implicit method. It generates the principal coordinates $q_j(t)$, which are multiplied by the corresponding mode-shapes $\Phi_j(x)$ to generate the flexural deflection $z(x,t)$. The bending moment is generated by the moment–curvature relation as:

$$M(x,t) = \sum_{j=1}^{\infty} \mathrm{EI}(x) \Phi_j''(x) q_j(t) \tag{22}$$

and the tensile stress at deck/keel is the bending moment divided by the section modulus, i.e.,

$$\sigma_{xx}(x,t) = \frac{\sum_{j=1}^{\infty} EI(x) \Phi_j''(x) q_j(t)}{I(x)} \cdot Z_{\text{deck/keel}}, \tag{23}$$

where $Z_{\text{deck/keel}}$ is the distance of the deck/keel from the horizontal neutral axis. The shear force is evaluated as:

$$V(x,t) = \sum_{j=1}^{\infty} EI(x) \Phi_j'''(x) q_j(t). \tag{24}$$

The shear stress at a given station is

$$\tau_{zx}(x,z,t) = \frac{V(x,t)Q(z)}{I(x)b(z)} \tag{25}$$

where $Q(z)$ is the first moment of area beyond 'z' away from the horizontal NA, and $b(z)$ is the local breadth.

Figure 7 shows the wave-induced hull girder vertical bending moment for sea state 7. The bending moment is maximum amid ships and zero at the ends. It shows the superposition due to several wave frequencies, especially whose wavelengths are close to the length of the hull. This is the springing behavior, which causes alternate compressive and tensile stresses on the deck and the keel plates of the hull. The shear force is zero amidships, and at the ends; while it is maximum at $x \sim L/4$, $3L/4$. The shear stress is maximum at the neutral axis and zero at the deck/keel plates.

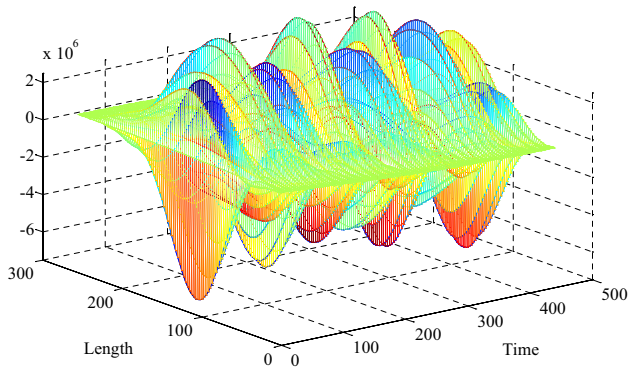

Fig. 7 Bending moment ($N-m$) of containership, sea state 7 (Wind speed = 14–17 m/s, $H_{1/3}$ = 4–5.5 m)

3.3.2 Frequency domain analysis

The excitation force is a function of the excitation frequency ω_e, and so is the response $z(x,t)$. The maximum deflection, bending moment $M(x,t)$, and shear force $V(x,t)$, corresponding to each frequency is plotted as function of ω_e. The tensile and the shear stress spectra follow. The area under each spectrum gives the RMS value.

The Rayleigh probability distribution of the stress amplitudes is generated by

$$p(\sigma_{amp}) = \frac{2\sigma_{amp}}{\sigma^2_{rms}} \exp\left\{-\frac{\sigma^2_{amp}}{\sigma^2_{rms}}\right\}. \tag{26}$$

Given the sea state, the number of waves encountered, N, is known from the average zero-up crossing period. The most probable largest stress amplitude is given by $\sigma_{1/N} = \sigma_{rms}\sqrt{2\ln(N)}$. This is repeated for the shear stress.

4 Results

The head-sea condition stretches the sea spectrum into higher frequencies, and changes the time-scale of the excitation. Following sea compresses the spectrum to very low frequencies, where springing is extremely unlikely. The apparent encounter frequency (using the deep water dispersion relation) is expressed as :

$$\omega_{enc} = \omega_e - \frac{\omega_e^2 V}{g}\cos\theta, \tag{27}$$

where V is the forward speed of the ship and θ is the heading angle, i.e., the angle between the ship velocity vector and the wave propagation direction. For head sea, the heading angle is $\theta = 180°$, i.e., encounter frequency is $\omega_{enc} = \omega_e + \omega_e^2 V/g$. The ship apparently experiences higher frequencies. For sea state 7, the average wind speed is 15.5 m/sec, the spectral speak frequency is $\omega_{peak} = \frac{0.877g}{U_{wind}} = 0.56\ \frac{rad}{s}$. For a forward speed of 16 knots (= 16 × 0.5144 = 8.23 m/s), the apparent peak frequency becomes 0.81 rad/s. For a forward speed of 25 knots (= 16 × 0.5144 = 12.86 m/s), the apparent peak frequency becomes 0.96 rad/s.

The sea spectrum ordinate $S(\omega_{enc})$ is stretched to the apparent higher frequencies, but is reduced in magnitude. The total energy content of the sea remains constant, i.e., $\int_0^\infty S(\omega_e)d\omega_e = \int_0^\infty S(\omega_{enc})d\omega_{enc}$.. Thus the encounter sea spectrum ordinate is expressed as

$$S(\omega_{enc}) = \frac{S(\omega_e)}{\left(\frac{d\omega_{enc}}{d\omega_e}\right)} = \frac{S(\omega_e)}{(1+2\omega_e V/g)}. \tag{28}$$

Indian merchant ships use steel grade IS-2062(A), whose yield tensile stress $\sigma_{yield} = 250$ MPa and yield shear stress $\tau_{yield} = 125$ MPa. The two hulls have been subjected to random wave loads at sea states 3 and 7. The sea is stationary, ergodic, and has a zero mean (i.e., no swell). Assuming a 3-h period of a given sea state, duration = 3 × 60 × 60 = 10800s. Thus $N = \frac{\text{duration}}{T_z}$, where $T_z = 2\pi\sqrt{\frac{m_0}{m_2}}$ is the average zero-up crossing period.

- For sea-state 3, wind-speed = 2.4 m/s, $H_{1/3} = 0.4085$ m, $T_z = 6.317$ s, $N = 1710$.
- For sea-state 7, wind-speed = 15.5 m/s, $H_{1/3} = 5.088$ m, $T_z = 9.524$ s, $N = 1134$.

All calculations in Sect. 3 are repeated. The springing added mass is speed-independent [1]. The response spectrum at sea-state 7, in terms of $z(x,t)$, $\sigma_{xx}(x,t)$, and $\tau_{zx}(x,t)$ have been plotted in Fig. 8a–c, respectively, for both hulls and two speeds, against the circular wave frequency ω_e. The container has a design speed of 25 knots, and the tanker has a design speed as 16 knots. The maximum and the RMS of these quantities have been tabulated at three sea states (Table 5), and their most probable largest amplitudes have also been estimated.

As sea state increases, the maximum deflection and stresses increase in magnitude; and their spectra spread over a larger range of excitation frequencies. Higher sea states make the sea spectrum heavier on the lower frequencies. Forward speeds stretch the response spectra to higher frequencies. The containership is seen to suffer larger stresses than the tanker. The greater mass and added mass of the tanker makes it tender, leading to lower response amplitudes and dynamic stress levels. The containership is more prone to springing excitation, especially at higher forward speeds, where the maximum stress spectral ordinate

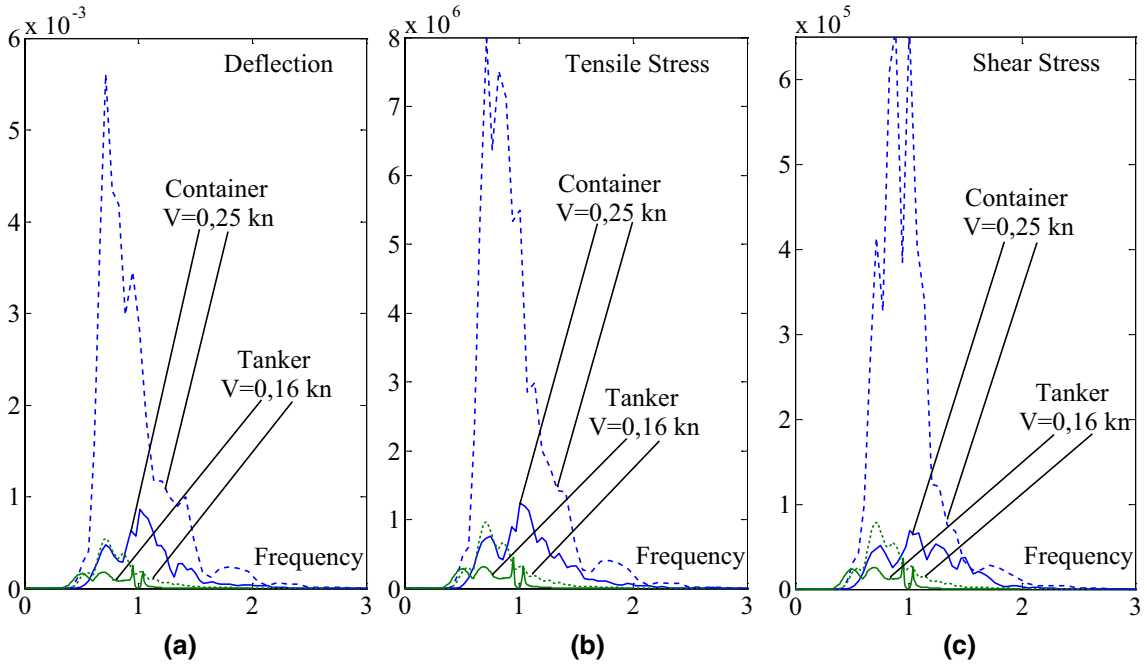

Fig. 8 **a** Flexural response spectrum. **b** Tensile stress spectrum. **c** Shear stress spectrum (SS7)

Table 5 Response characteristics of two hulls in different sea states (SS) with zero and non-zero forward speeds

Sea state	Container ship V = 0		Tanker V = 0	Container ship = 25 knots		Tanker = 16 knots
	3	7	7	3	7	7
Max z (m)	3.22×10^{-6}	0.00087	0.00025	14×10^{-6}	0.0056	0.00054
Max σ_{xx} (Pa)	7.47×10^{3}	1.25×10^{6}	4.47×10^{5}	3.4×10^{4}	8.03×10^{6}	9.61×10^{6}
Max τ_{zx} (Pa)	5.6×10^{2}	6.91×10^{4}	3.65×10^{4}	5.48×10^{3}	6.62×10^{5}	7.87×10^{4}
z^2_{rms} (m^2)	2.8×10^{-6}	0.00028	0.000089	2.3×10^{-5}	0.0023	0.0002
σ^2_{rms} (Pa^2)	6.45×10^{3}	4.57×10^{5}	1.43×10^{5}	6.81×10^{4}	3.94×10^{6}	3.65×10^{5}
τ^2_{rms} (Pa^2)	4.94×10^{2}	3.14×10^{4}	1.18×10^{4}	8.82×10^{3}	3.04×10^{5}	3.00×10^{4}
$\sigma_{1/N}$ (3 h) (Pa)	204.18	1663.60	936.51	663.78	4906.72	1493.13
$\tau_{1/N}$ (3 h) (Pa)	56.54	438.19	268.28	238.80	1361.92	428.14

becomes several times of that at zero forward speed. The wavelength (equaling the ship length) which causes the maximum bending moments; corresponds to a wave frequency of ~0.5 rad/s, which corresponds to a non-negligible wave amplitude, thereby inducing springing. The very low structural damping of steel causes this flexural behavior to reach large amplitudes at the resonant excitation frequencies. A mere structural damping of $<5\%$ causes the dynamic amplitudes to be at least ten times of the static response.

5 Discussion and conclusions

A non-uniform hull girder is mathematically generated, with a non-analytical (arbitrary) variation of the sectional mass and flexural rigidity. It is modeled as non-uniform Euler–Bernoulli beam for free and forced wet vibration analysis. The free vibration frequencies and modeshapes have been generated using the energy-based Rayleigh–Ritz method, by superposition of the closed-form (analytical) uniform beam modeshapes. About 3–4 uniform beam modeshapes need to be superposed, to generate the convergent non-uniform modeshape. This eases the process of generation of non-uniform frequency and modeshape, as compared to FEA. The lower the order of the rectellipsoid in the benchmark cases, the more the non-uniform modeshape deviates from the uniform beam modeshape. A very high order of the rectellipsoid generates almost a cuboid, which behaves like a uniform beam. The ease of modelling a very wide range of section shapes of merchant vessels using only four section parameters $(a(x), b(x), p(x), q(x))$, show the versatility of this closed-form mathematical

approach. The subsequent hull form can be conveniently analyzed. Closed-form analytical expressions exist for structural area, neutral axis height, second moment of area in horizontal and vertical bending, polar moment of inertia etc. This also eases the evaluation of sectional added mass and damping coefficients, bypassing the computationally expensive source distribution technique. This becomes handy for preliminary estimation of hull frequencies. Storage of shapes and underwater geometry is much easier, because we require only four parameters to store a curve. Such reasonably accurate representations of underwater geometry help to conveniently model the arbitrary mass and stiffness distributions over the length of the hull. The import and export of the sections from software to another requires less memory and time.

Utilizing the strip theory, the 2D Green's function technique has been used to generate the radiation potential. The use of the auxiliary radiation potential, which is only a function of space, shows the total radiation force to be in phase with flexural acceleration of the body. This leads to the wet natural frequencies of the hull girder. The high-frequency limit of the free-surface boundary condition leads to negligible radiation damping. The frequency reduction due to inclusion of fluid inertia is the highest for the fundamental mode, and decreases consistently for higher modes.

The wave excitation is modeled as fully developed sea, obeying the Pierson–Moskowitz spectrum. The Froude–Krylov hydrodynamic pressure is modified due to the presence of the vessel, giving rise to a diffraction potential. Using the Haskind's relations, the radiation–diffraction problem has been established. Modal superposition method is used to generate the flexural response in the frequency domain. The individual responses to sinusoidal wave excitation can be superposed assuming linear wave theory and linear structural behavior.

The excitation spectrum for vertical vibration can be generated by integrating the excitation hydrodynamic pressure over the wetted surface area of the hull in the vertical direction. This spectrum depends on the sea state and the encounter frequency. Each vessel has a frequency-dependent transfer function, which depends on its own properties like mass, stiffness, radiation force coefficients, and structural damping. The product of the excitation spectrum and the transfer function gives the response spectrum, which is narrow-banded. Short-term extreme responses are predicted from the response spectra of the two hulls at two different forward speeds. Structural design recommendations can be drawn from the response spectra. Given a safety factor of 3, the extreme stress level should not exceed 1/3rd the magnitude of the yield stress.

References

1. A.W. Troesch, Wave-induced hull vibrations: an experimental and theoretical study. J. Ship Res. **28**(2), 141–150 (1984)
2. J.N. Newman, "Deformable floating bodies", in *Proceedings of 8th International Workshop on Water Waves and Floating Bodies*", Newfoundland (1993)
3. J.N. Newman, Wave effects on deformable bodies. Appl. Ocean Res. **16**, 47–59 (1994)
4. J.J. Jensen, Wave-induced ship hull vibrations in stochastic seaways. Mar. Struct. 9, 353–387 (1996)
5. J. Jung, Y. Park, H. Shin, I. Park, A. Korobkin, "An estimation of hull girder response due to wave excitation", in *Proceedings of the 13th International Offshore and Polar Engineering Conference, Hawaii, USA*, (2003)
6. M. Wu, T. Moan, Efficient calculation of wave-induced ship responses considering structural dynamic effects. Appl. Ocean Res. **27**, 81–96 (2005)
7. Y. Kim, K. Kim, Y. Kim, Springing analysis of a seagoing vessel using a fully coupled BEM-FEM in the time-domain. Ocean Eng. **36**, 785–796 (2009)
8. S. Zhu, M. Wu, T. Moan, Experimental investigation of hull girder vibrations of a flexible backbone model in bending and torsion. Appl. Ocean Res. **33**, 252–274 (2011)
9. S. Timoshenko, *Vibration Problems in Engineering*, 2nd edn. (D. Van Nostrand Company INC., New York, 1937)
10. N. Datta, J.D. Thekinen, A Rayleigh-Ritz based approach to characterize the vertical vibration of non-uniform hull girder. Ocean Eng. **125**, 113–123 (2016)
11. J.N. Newman, *Marine Hydrodynamics* (MIT Press, Cambridge, 1977)